

## Research Paper

## A novel nonlinear solution for the polygon scaled boundary finite element method and its application to geotechnical structures

Kai Chen<sup>a,b</sup>, Degao Zou<sup>a,b,\*</sup>, Xianjing Kong<sup>a,b</sup>, Andrew Chan<sup>c</sup>, Zhiqiang Hu<sup>a,b</sup><sup>a</sup> The State Key Laboratory of Coastal and Offshore Engineering, Dalian University of Technology, Dalian, Liaoning 116024, China<sup>b</sup> School of Hydraulic Engineering, Dalian University of Technology, Dalian, Liaoning 116024, China<sup>c</sup> School of Engineering and ICT, University of Tasmania, Australia

## ARTICLE INFO

## Article history:

Received 28 June 2016

Received in revised form 26 September 2016

Accepted 27 September 2016

## Keywords:

Polygon element

Elasto-plastic

Scaled boundary finite element

Finite element method

## ABSTRACT

The polygon scaled boundary finite element method is semi-analytical and known for its high precision. However, the material nonlinearity cannot be maintained because this method uses an analytical solution in the radial direction. In this paper, a novel nonlinear algorithm is developed by introducing internal Gaussian points over a subdomain. The response of nonlinearity for a concrete-faced rockfill dam is modeled. The results correspond well with the results from finite element modelling, which demonstrates the method can be used to describe the nonlinear characteristics of geomaterials. Furthermore, this method offers promising flexibility for analyzing complex geometries without decreasing the precision.

© 2016 Elsevier Ltd. All rights reserved.

## 1. Introduction

Material nonlinearity is an inevitable problem in the numerical simulations of many engineering structures. Many researchers are interested in studying and implementing nonlinear calculation methods and software. The finite element method (FEM) has been used extensively as an effective technique for obtaining reasonable solutions. In traditional FEM, the domain is often discretized into triangles or quadrilaterals. Polygon finite elements and related methods have been proposed in recent years. Some representative numerical methods are based on polygon elements, such as the rational function interpolation by Wachspress [1–3], the Voronoi cell finite element method (VCFEM) and polygon elements using natural neighbor shape functions [4,5], the planar arbitrary polygonal element method [6,7], the macro-element Galerkin method (MEGM) [8], the conforming polygonal finite element (CPFE) method [9] and the natural element method (NEM) [10]. Using polygon elements, the discretization becomes more flexible, offering high accuracy and a high degree of convergence, and the mechanical properties can be simulated conveniently and effectively. The aforementioned methods based on polygon finite elements [11–13] are promising in the numerical simulation field.

The scaled boundary finite element method (SBFEM), presented by Wolf and Song [14–17], combines the advantages of the boundary element method (BEM) and FEM. SBFEM is a semi-analytical method, in which a numerical solution is obtained in the circumferential direction and an analytical value can be derived in the radial direction. Compared with conventional FEM, SBFEM increases the degree of precision and convergence in the numerical simulations and significantly reduces the number of degrees of freedom in the computational model. In addition, no fundamental solutions are required for the application of the variational principle. These advantages/benefits make SBFEM a powerful tool for a wide variety of linear elasticity problems.

During the past two decades, SBFEM has been used to many problems in engineering fields, such as those related to unbounded media [18], electrostatic fields [19], electromagnetic waveguides [20], magneto-electro-elastic plates [21] and fluid-structure interactions [22]. In unbounded media, the radiation conditions at infinity can be satisfied exactly and automatically. The number of elements is dramatically reduced in the fluid-structure interaction field because discretization is only performed at the boundary. In electromagnetic problems, the singularity of the contact between different materials can be efficiently solved.

The polygonal scaled boundary finite element method (PSBFEM) was recently developed based on SBFEM. The concept of polygons was introduced to handle more complex geometries, making SBFEM more flexible and convenient. Compared with

\* Corresponding author at: The State Key Laboratory of Coastal and Offshore Engineering, Dalian University of Technology, Dalian, Liaoning 116024, China.

E-mail address: [zoudegao@dlut.edu.cn](mailto:zoudegao@dlut.edu.cn) (D. Zou).

FEMs, PSBFEM contributes to getting a higher degree of precision and convergence [23]. Many researchers have implemented PSBFEM through numerical simulation. Ooi [24–27] applied this theory to solve the fracture analysis of structures; Bao [28] simulated the crack propagation of a gravity dam under seismic loading; and Mingguang [29] modeled the crack propagation for contacts between different materials.

However, SBFEM are mostly subject to linear elastic materials and rarely used in non-linearity materials in practice, especially in engineering fields. Combining SBFEM with the homotopy analysis method (HAM), Lin and Liao [30] applied SBFEM to solve non-linear problems. The least squares method was introduced to adjust to the integration polynomial to simulate plasticity over each polygon, and the PSBFEM formulation for elasto-plastic analysis was derived by Ooi et al. [31]. This study presents a different approach for applying SBFEM to non-linear materials.

According to the integral rule of triangles in FEM, three internal Gaussian integration points are introduced over a sector covered by a line element on the boundary, and a novel nonlinear polygon scaled boundary finite element method (NPSBFEM) is developed to simulate the nonlinear properties of geomaterials. The elasto-plastic constitutive matrix, stiffness matrix and imbalance force vector can be conveniently derived by combining the development platform of the finite element procedure. Then, SBFEM can be used to model nonlinear material properties with polygon elements.

The remainder of this paper is organized as follows. The basic theoretical derivation of the PSBFEM is introduced in Section 2. The displacement field, the shape function of the polygon elements and the incremental strain and stress fields are also described in Section 2. Section 3 describes the scaled boundary polygon formulation for elasto-plastic analysis. The development platform of the proposed algorithm is introduced in Section 4. The reliability of the procedure is validated by two numerical examples in Section 5. Section 6 summarizes the major conclusions that can be drawn from this study.

## 2. Theoretical derivation of the PSBFEM

### 2.1. Coordinate transformation

An arbitrary domain  $\Omega$  can be discretized with a mesh of arbitrary  $n$ -sided polygons (where  $n$  can be any integer  $\geq 3$ ). Any polygon can be treated as an SBFEM subdomain as long as its geometry satisfies the SBFEM scaling requirement, i.e., any point on the polygon boundary must be directly visible from the scaling center. The numerical results of the domain are obtained after solving each subdomain with the SBFEM.

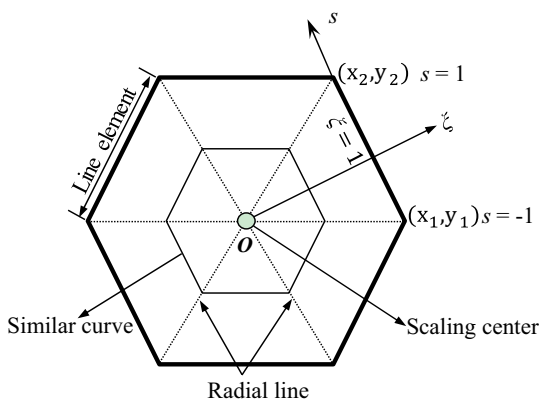


Fig. 1. Polygon representation of the SBFEM.

Fig. 1 shows a typical polygon modeled using the PSBFEM. A scaling center is defined at the geometric center of the polygon. Each edge on the polygon is discretized using one-dimensional line elements with a local coordinate  $s$  that varies from  $-1$  to  $+1$ , and a radial coordinate  $\xi$  is defined that varies from zero at the scaling center to unity on the boundary. Two-node linear elements are used in this study; the Cartesian coordinates of an element can be expressed in terms of the scaled boundary coordinates as follows:

$$\mathbf{x}_b(s) = \mathbf{N}(s)\mathbf{x}_b \quad (2-1)$$

$$\mathbf{y}_b(s) = \mathbf{N}(s)\mathbf{y}_b \quad (2-2)$$

$$\mathbf{N}(s) = [N_1(s), N_2(s), N_3(s), \dots, N_m(s)] \quad (2-3)$$

where  $\mathbf{x}_b$  and  $\mathbf{y}_b$  represent the vector of nodal coordinates on the boundary,  $\mathbf{x}_b(s)$  and  $\mathbf{y}_b(s)$  are the coordinate vectors along the line element, and  $\mathbf{N}(s)$  is the shape function vector of a line element with  $m$  nodes on the polygon boundary. Only the boundary is discretized with line elements in each subdomain of SBFEM, so increasing the order of the shape function does not increase the mesh complexity. Increasing the order of the shape functions is convenient if necessary, and standard one-dimensional Gauss-Lobatto-Lagrange shape functions can be used. The entire polygon domain can be captured by scaling the polygon boundaries according to the radial coordinate with respect to the scaling center  $O$ . The scaled boundary coordinate system  $(\xi, s)$  is related to the Cartesian coordinate system by the scaling equation as follows:

$$x(\xi, s) = \xi \mathbf{N}(s)\mathbf{x}_b \quad (2-4)$$

$$y(\xi, s) = \xi \mathbf{N}(s)\mathbf{y}_b \quad (2-5)$$

where  $(x, y)$  is the geometry of a point inside the domain.

### 2.2. Scaled boundary polygon shape functions

For a sector covered by a line element on a polygon boundary, an approximate solution for the displacement at any point in a subdomain can be written in a form related to the local coordinates of the SBFEM:

$$\mathbf{u}(\xi, s) = \mathbf{N}_u(s)\mathbf{u}(\xi) \quad (2-6)$$

where the nodal displacement functions  $\mathbf{u}(\xi)$  are introduced, which denote the displacements along the radial lines are analyzed with respect to the radial coordinate, and  $\mathbf{N}_u(s)$  represents the shape function matrix, which has the following form:

$$\mathbf{N}_u(s) = \begin{bmatrix} N_1(s) & 0 & N_2(s) & 0 & \cdots & 0 & N_m(s) & 0 \\ 0 & N_1(s) & 0 & N_2(s) & 0 & \cdots & 0 & N_m(s) \end{bmatrix} \quad (2-7)$$

Then, the partial differential equations of equilibrium for a polygon derived from the Galerkin weighted residual method result in the following equation, and the radial displacement functions  $\mathbf{u}(\xi)$  are the solution to the SBFEM governing equation for displacement.

$$\mathbf{E}_0 \xi^2 \mathbf{u}(\xi)_{,\xi\xi} + (\mathbf{E}_0 - \mathbf{E}_1 + \mathbf{E}_1^T) \xi \mathbf{u}(\xi)_{,\xi} - \mathbf{E}_2 \mathbf{u}(\xi) + \mathbf{F}(\xi) = 0 \quad (2-8)$$

where the coefficient matrices  $\mathbf{E}_i (i = 0, 1, 2)$  depend only on the geometry and material properties of the subdomain, which are evaluated for line elements and assembled over the discretized polygon boundary, and  $\mathbf{F}(\xi)$  is a load vector that includes contributions from side-face traction, body and thermal loads. Introducing a new vector  $\mathbf{X}(\xi)$  when the load vector  $\mathbf{F}(\xi)$  becomes zero transforms Eqs. (2-8) into a first-order homogeneous differential equation system with respect to  $\xi$ :

$$\mathbf{X}(\xi) = \begin{Bmatrix} \mathbf{u}(\xi) \\ \mathbf{q}(\xi) \end{Bmatrix} \quad (2-9)$$

$$\xi \mathbf{X}(\xi)_{,\xi} = -\mathbf{Z} \mathbf{X}(\xi) \quad (2-10)$$

The coefficient matrix  $\mathbf{Z}$  is a typical Hamiltonian matrix, as expressed in Eq. (2-11),  $\mathbf{q}(\xi)$  is the internal nodal force vector, and  $\mathbf{u}(\xi)$  is the corresponding displacement vector along the  $\xi$ -direction.

$$\mathbf{Z} = \begin{bmatrix} \mathbf{E}_0^{-1} \mathbf{E}_1^T & -\mathbf{E}_0^{-1} \\ \mathbf{E}_1 \mathbf{E}_0^{-1} \mathbf{E}_1^T - \mathbf{E}_2 & -\mathbf{E}_1 \mathbf{E}_0^{-1} \end{bmatrix} \quad (2-11)$$

Using eigenvalue decomposition, the matrix  $\mathbf{Z}$  can be decoupled into pairs of eigenvalues of  $\lambda_i$  and  $-\lambda_i$ , and the standard eigenvalue problem necessary for a polygon is formulated as

$$\mathbf{Z} \begin{bmatrix} \psi_u \\ \psi_q \end{bmatrix} = \begin{bmatrix} \psi_u \\ \psi_q \end{bmatrix} \mathbf{S}_n \quad (2-12)$$

where the diagonal entries of  $\mathbf{S}_n$  are composed of the real parts of the eigenvalues. The entries include two zeros (representing the two modes of translational rigid body motion) and negative numbers. The parameters  $\psi_u$  and  $\psi_q$  are modal displacements and forces, respectively, depending on the DOFs of the line elements. For a bounded polygon, the solution to Eq. (2-8) can be formulated as

$$\mathbf{u}(\xi) = \psi_u \xi^{-\mathbf{S}_n} \mathbf{c}_n \quad (2-13a)$$

$$\mathbf{q}(\xi) = \psi_q \xi^{-\mathbf{S}_n} \mathbf{c}_n \quad (2-13b)$$

where the coefficients  $\mathbf{c}_n$  are integration constants, which can be determined from the nodal displacement vector on the subdomain boundary  $\mathbf{u}_b = \mathbf{u}(\xi = 1)$ :

$$\mathbf{c}_n = \psi_u^{-1} \mathbf{u}_b \quad (2-14)$$

The general solutions for displacements  $\mathbf{u}(\xi)$  and nodal internal forces  $\mathbf{q}(\xi)$  are obtained by substituting Eq. (2-14) into Eq. (2-13):

$$\mathbf{u}(\xi) = \psi_u \xi^{-\mathbf{S}_n} \psi_u^{-1} \mathbf{u}_b \quad (2-15a)$$

$$\mathbf{q}(\xi) = \psi_q \xi^{-\mathbf{S}_n} \psi_u^{-1} \mathbf{u}_b \quad (2-15b)$$

Then, the displacement field  $\mathbf{u}(\xi, s)$  in a sector covered by a line element on the polygon boundary is evaluated by substituting Eq. (2-15a) into Eq. (2-6) (see Fig. 1) and can be expressed in terms of  $\mathbf{u}_b$  as

$$\mathbf{u}(\xi, s) = \mathbf{N}_u(s) \psi_u \xi^{-\mathbf{S}_n} \psi_u^{-1} \mathbf{u}_b \quad (2-16)$$

Therefore, the polygon element shape functions  $\Phi(\xi, s)$ , similar to FEM, are extracted as

$$\Phi(\xi, s) = \mathbf{N}_u(s) \psi_u \xi^{-\mathbf{S}_n} \psi_u^{-1} \mathbf{u}_b \quad (2-17)$$

The strain field formulation in SBFEM was proposed by Wolf [14]. Substituting the displacement function  $\mathbf{u}(\xi)$ , the strain-displacement matrix [14]  $\mathbf{B}(\xi, s)$  is

$$\boldsymbol{\varepsilon}(\xi, s) = \mathbf{B}_1(s) \mathbf{u}(\xi)_{,\xi} + \xi^{-1} \mathbf{B}_2(s) \mathbf{u}(\xi) \quad (2-18)$$

$$\boldsymbol{\varepsilon}(\xi, s) = [\mathbf{B}_1(s) \psi_u [-\mathbf{S}_n] + \mathbf{B}_2(s) \psi_u] \xi^{-\mathbf{S}_n-1} \psi_u^{-1} \mathbf{u}_b \quad (2-19)$$

$$\mathbf{B}(\xi, s) = [\mathbf{B}_1(s) \psi_u [-\mathbf{S}_n] + \mathbf{B}_2(s) \psi_u] \xi^{-\mathbf{S}_n-1} \psi_u^{-1} \quad (2-20)$$

where  $\mathbf{B}_1(s)$  and  $\mathbf{B}_2(s)$  are transformation coefficient matrices that are expressed as follows:

$$\mathbf{B}_1(s) = \frac{1}{|J(s)|} \begin{bmatrix} y_b(s)_{,s} & 0 \\ 0 & -x_b(s)_{,s} \\ -x_b(s)_{,s} & y_b(s)_{,s} \end{bmatrix} \mathbf{N}_u(s) \quad (2-21)$$

$$\mathbf{B}_2(s) = \frac{1}{|J(s)|} \begin{bmatrix} -y_b(s)_{,s} & 0 \\ 0 & x_b(s)_{,s} \\ x_b(s)_{,s} & -y_b(s)_{,s} \end{bmatrix} \mathbf{N}_u(s) \quad (2-22)$$

Then, the strain fields of the scaled boundary finite element in elasto-plastic analysis can be simplified as shown in Eq. (2-23):

$$\boldsymbol{\varepsilon}(\xi, s) = \mathbf{B}(\xi, s) \mathbf{u}_b \quad (2-23)$$

The incremental strain field can be decomposed into elastic and plastic strain incremental components. The plastic strain increment can be determined from the plastic flow rule. Assuming associative plasticity and using the yielding functions  $F$  and the plastic multiplier  $\Delta\lambda$ , the plastic strain increment is formulated as shown in Eq. (2-25):

$$\Delta \boldsymbol{\varepsilon} = \Delta \boldsymbol{\varepsilon}_e + \Delta \boldsymbol{\varepsilon}_p \quad (2-24)$$

$$\Delta \boldsymbol{\varepsilon}_p = \frac{\partial F}{\partial \boldsymbol{\sigma}} \Delta \lambda \quad (2-25)$$

where  $F = F(\boldsymbol{\sigma}, \kappa)$  is defined as the yield function in the formula and is determined by the current stress state  $\boldsymbol{\sigma}$  and the hardening parameter  $\kappa$ .

Using Hooke's law and substituting Eq. (2-25) into Eq. (2-24), the incremental stress field  $\Delta \boldsymbol{\sigma}$  can be written as

$$\Delta \boldsymbol{\sigma} = \mathbf{D}_{ep} \Delta \boldsymbol{\varepsilon} \quad (2-26)$$

where  $\mathbf{D}_{ep}$  is the elasto-plastic constitutive matrix, and the formula of the generalized plasticity model [32,33] is

$$\mathbf{D}_{ep} = \mathbf{D}^e - \frac{\mathbf{D}^e : \mathbf{n}_{gL/U} \otimes \mathbf{n} : \mathbf{D}^e}{H_{L/U} + \mathbf{n} : \mathbf{D}^e : \mathbf{n}_{gL/U}} \quad (2-27)$$

The subscripts  $L$  and  $U$  denote load and unload, respectively,  $\mathbf{D}^e$  is the elastic constitutive matrix,  $\mathbf{n}$  is the loading direction vector,  $\mathbf{n}_g$  is the flow direction vector, and  $H$  is the plastic modulus; the remaining definitions are provided in Appendix A.

The distinction between the loading and unloading directions is described using the following criteria:

$$\mathbf{n} : d\boldsymbol{\sigma}^e > 0 \quad (\text{loading}) \quad (2-28a)$$

$$\mathbf{n} : d\boldsymbol{\sigma}^e < 0 \quad (\text{unloading}) \quad (2-28b)$$

where  $d\boldsymbol{\sigma}^e$  is the elastic stress increment. Substituting Eq. (2-27) and (2-23) into Eq. (2-26) enables expressing the incremental stress field as

$$\Delta \boldsymbol{\sigma}(\xi, s) = \mathbf{D}_{ep} \mathbf{B}(\xi, s) \Delta \mathbf{u}_b \quad (2-29)$$

where  $\Delta \mathbf{u}_b$  is the nodal displacement increment.

### 3. Polygon formulation-based SBFEM for elasto-plastic analysis

When the nodal displacements are solved using SBFEM, the displacement field over the discretized subdomain can be easily interpolated. Similar to FEM, the scaled boundary polygon formulation for elasto-plasticity can be derived by applying the principle of virtual work, which is written in SBFEM coordinates as

$$\int_{\Omega} \delta \boldsymbol{\varepsilon}^T \Delta \boldsymbol{\sigma}(\xi, s) d\Omega = \int_{\Gamma} \delta \mathbf{u}^T \mathbf{f}_t d\Gamma + \int_{\Gamma} \delta \mathbf{u}^T \mathbf{f}_b d\Gamma - \int_{\Omega} \delta \boldsymbol{\varepsilon}^T \boldsymbol{\sigma}(\xi, s) d\Omega \quad (3-1)$$

where  $\Delta \boldsymbol{\sigma}(\xi, s)$  is the incremental stress field,  $\mathbf{f}_t$  and  $\mathbf{f}_b$  are the surface traction and body force intensity, respectively, and  $\delta \boldsymbol{\varepsilon}(\xi, s)$  is

the virtual strain field corresponding to the virtual displacement field  $\delta \mathbf{u}(\xi, s)$ . Substituting the variables as defined in the previous sections, the simplified version of Eq. (3-1) can be expressed as

$$\left( \int_{\Omega} \mathbf{B}^T(\xi, s) \mathbf{D}_{ep} \mathbf{B}(\xi, s) d\Omega \right) \Delta \mathbf{u}_b = \left( \int_{\Gamma} \Phi^T(\xi, s) \mathbf{f}_t d\Gamma + \int_{\Gamma} \Phi^T(\xi, s) \mathbf{f}_b d\Omega \right) - \left( \int_{\Omega} \mathbf{B}^T(\xi, s) \boldsymbol{\sigma}(\xi, s) d\Omega \right) \quad (3-2)$$

The term within the first set of parentheses on the left-hand side of Eq. (3-2) is the elasto-plastic stiffness matrix of the polygon  $\mathbf{K}_{ep}$ , the term within the second set of parentheses is the external load vector  $\mathbf{R}_{ext}$ , and the term within the third set of parentheses is the internal load vector  $\mathbf{R}_{int}$ . Eq. (3-2) can be simplified as

$$\mathbf{K}_{ep} \Delta \mathbf{u}_b = \mathbf{R}_{ext} - \mathbf{R}_{int} \quad (3-3)$$

Similar to conventional FEM, Eq. (3-3) is a system of nonlinear equilibrium equations that can be assembled polygon by polygon. Then, the total equilibrium equation of the discretized domain is described as

$$\left( \sum_{i=1}^{nPol} \mathbf{K}_{ep} \right) \Delta \mathbf{U}_b = \sum_{i=1}^{nPol} (\mathbf{R}_{ext} - \mathbf{R}_{int}) \quad (3-4)$$

where  $\Delta \mathbf{U}_b$  is the incremental nodal displacement vector on the boundary of the entire domain. Standard nonlinear iterative procedures, such as the modified Newton-Raphson iterations, can be used to solve this equation.

### 3.1. Elasto-plastic constitutive matrix

The formula of the constitutive matrix was derived in the previous section, but another approach is used to evaluate the matrix in this study. Ooi et al. [31] applied a polynomial in terms of scaled boundary coordinates  $(\xi, s)$  to approximate  $\mathbf{D}_{ep}$ , which is first expressed as Eqs. (3-5) with Cartesian coordinates  $(x, y)$  and is then transformed into the SBFEM coordinates:

$$\mathbf{D}_{ep}(x, y) = \mathbf{D}_0 + \mathbf{D}_1 x + \mathbf{D}_2 y + \mathbf{D}_3 x^2 + \mathbf{D}_4 xy + \mathbf{D}_5 y^2 + \dots \quad (3-5)$$

where the coefficient matrices  $\mathbf{D}_i$ ,  $i = 0, 1, 2, \dots$  are determined by a least squares fit over each polygon. The Gaussian integration points of the line can be used for this purpose. Additional fitting points along the  $\xi$  coordinate can also be included to compute the fitting function if necessary, and the points are shown in Fig. 2. This assumption requires polygons that are sufficiently small for the variation of  $\mathbf{D}_{ep}$  in the plastic zone to be represented accurately, and it is relatively computationally intensive.

The conventional finite element theory is used to evaluate the elasto-plastic constitutive matrix  $\mathbf{D}_{ep}$  in this paper. First, a sector covered by a line element is taken as a triangular element. Then, three Gaussian integration points are introduced into the element. The locations of the points are determined according to the integration rule of triangular elements; their positions in a polygon are shown in Fig. 3. The Gaussian points of the line are used to calculate the SBFEM coefficients, and the Gaussian points of the area are used for integration in the elasto-plastic analysis. For a polygon element with an arbitrary number of  $n$  sides, the number of Gaussian points of the area is  $3n$ , and the number of linear Gaussian points of the area is  $2n$ .

In conventional FEM, two-dimensional integrals on triangles are conveniently expressed in terms of triangular coordinates, as shown in Eq. (3-6), where  $(L_1^i, L_2^i, L_3^i)$  are the triangular coordinates of evaluation point  $i$ ,  $A_e$  is the area of triangle  $e$ ,  $m$  indicates the number of permutations associated with an evaluation point having a weight  $W_i$ , and  $E$  is the approximate error of the integration.

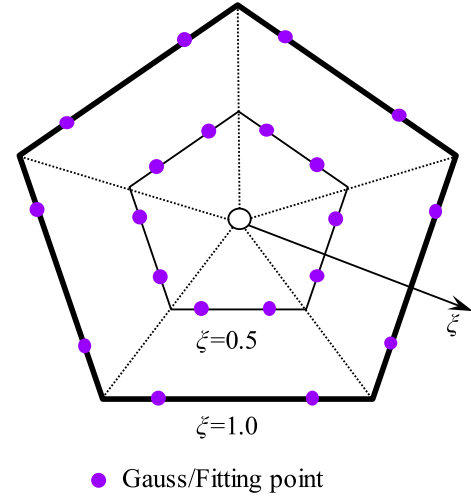


Fig. 2. Location of Gaussian points used to compute the fitting surfaces for  $\mathbf{D}(x, y)$  and  $\boldsymbol{\sigma}(x, y)$  for a polygon [31].

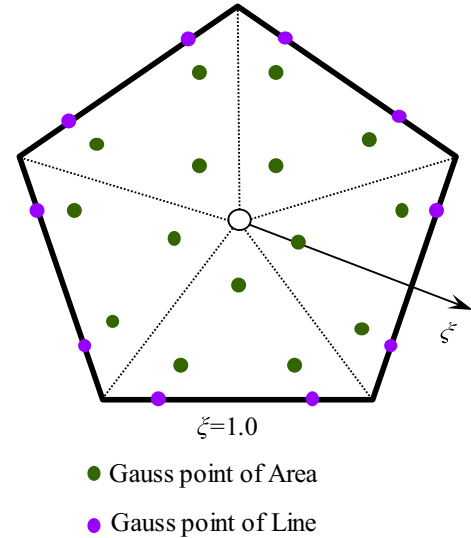


Fig. 3. Location of Gaussian points over a polygon element.

$$\iint_{\Omega_e} f(x, y) dx dy = A_e \sum_{i=1}^m W_i f(L_1^i, L_2^i, L_3^i) + E \quad (3-6)$$

The locations of the Gaussian points and the integration formulation for a standard triangular element are given as Eq. (3-7) when  $m$  is equal to three:

$$\iint_{\Omega_e} f(\xi, s) d\xi ds = \frac{1}{6} \left[ f\left(\frac{2}{3}, \frac{1}{6}, \frac{1}{6}\right) + f\left(\frac{1}{6}, \frac{1}{6}, \frac{2}{3}\right) + f\left(\frac{1}{6}, \frac{2}{3}, \frac{1}{6}\right) \right] + E \quad (3-7)$$

where the multiplicative factor arises because the area of the canonical element is  $1/2$  and all of the weights  $W_i$  are  $1/3$ .

### 3.2. Calculation of the elasto-plastic stiffness matrix

A polygon formulation of the elasto-plastic stiffness matrix can be derived from Eqs. (3-2) and (3-3) as follows:

$$\mathbf{K}_{ep} = \int_{\Omega} \mathbf{B}^T(\xi, s) \mathbf{D}_{ep} \mathbf{B}(\xi, s) d\Omega \quad (3-8)$$

Then, the polygon matrix  $\mathbf{K}_{ep}$  is determined by integrating over the discretized subdomain with the Gaussian points of area as follows:

$$\mathbf{K}_{ep} = \sum_{i=1}^{3n} \mathbf{B}^i(\xi, s) \mathbf{D}_{ep}^i \mathbf{B}^i(\xi, s) A_i \quad (3-9)$$

where  $\mathbf{B}^i(\xi, s)$  denotes the strain displacement transformation matrix determined by the  $i$ th Gaussian point and can be obtained using Eq. (2-20),  $\mathbf{D}_{ep}^i$  represents the constitutive elasto-plastic matrix of the  $i$ th Gaussian point, which is calculated from the generalized plasticity model [32,33], and  $A_i$  is the area held by the  $i$ th point in  $A_e$ . The elasto-plastic stiffness matrix of the discretized domain can be evaluated after each  $\mathbf{K}_{ep}$  has been determined for the polygons.

### 3.3. Calculation of the external load vector

The external load vector  $\mathbf{R}_{ext}$  can be extracted from Eq. (3-2) and is expressed as

$$\mathbf{R}_{ext} = \int_{\Gamma} \Phi^T(\xi, s) \mathbf{f}_t d\Gamma + \int_{\Omega} \Phi^T(\xi, s) \mathbf{f}_b d\Omega \quad (3-10)$$

The first term on the right-hand side of Eq. (3-10) is the distributed load on the boundary. This can be further simplified as follows when considering that at the polygon boundary ( $\xi = 1$ ),  $\Phi(\xi, s) = \mathbf{N}_u(s)$  applies:

$$\int_{\Gamma} \Phi^T(\xi, s) \mathbf{f}_t d\Gamma = \int_{-1}^1 \mathbf{N}_u(s) |\mathbf{J}(s)| \mathbf{f}_t ds \quad (3-11)$$

The second term is the body load vector. For the case of a constant body load, this term is expressed by substituting Eq. (2-17) and integrating numerically with the Gaussian points:

$$\int_{\Omega} \Phi^T(\xi, s) \mathbf{f}_b d\Omega = \sum_{k=1}^n \sum_{i=1}^3 [\mathbf{N}_u^i(s) \psi_u \xi_i^{-S_n} \psi_u^{-1}]^T \mathbf{f}_b A_{ki} \quad (3-12)$$

### 3.4. Calculation of the internal load vector

The formulation of the load vector because of the internal stresses is defined as Eq. (3-13), which is determined from Eq. (3-2). The stress distribution  $\sigma(\xi, s)$  was approximately evaluated using a polynomial function in the research of Ooi et al. [31], and the procedure is the same as that for  $\mathbf{D}_{ep}$ :

$$\mathbf{R}_{int} = \int_{\Omega} \mathbf{B}^T(\xi, s) \sigma(\xi, s) d\Omega \quad (3-13)$$

Here, numerical integration is introduced into the evaluation. First, the strain field  $\epsilon(\xi, s)$  can be calculated from Eqs. (2-20) and (2-23) after the nodal displacements  $\mathbf{U}_b$  on the boundary of the domain are known. Then, the stress field  $\sigma_i(\xi, s)$  at each Gaussian point is determined by substituting the elasto-plastic constitutive matrix  $\mathbf{D}_{ep}^i$ , and the formulas are expressed as

$$\mathbf{R}_{int} = \sum_{i=1}^{3n} \mathbf{B}^i(\xi, s)^T \sigma_i(\xi, s) A_i \quad (3-14)$$

$$\sigma_i(\xi, s) = \sum_{j=1}^{3n} \mathbf{D}_{ep}^i \epsilon_j(\xi, s) \quad (3-15)$$

## 4. Scaled boundary polygon procedure for elasto-plasticity

The polygon-scaled boundary finite elements method, PSBFEM\_Area (integrate over the area) with NPSBFEM and PSBFEM\_Line

(integrate on the boundary) are secondarily developed using object-oriented programming with Visual C++ based on the Windows software GEODYNA [34], which was developed by the second author. The scaled boundary polygon formulation is extended to static and dynamic elasto-plastic analyses of geotechnical engineering structures. The multi-core parallel technology is introduced into the GEODYNA program, which provides the computational capability for large-scale elasto-plastic analysis including millions of DOFs.

## 5. Numerical example

### 5.1. A cantilever beam analysis for elasticity

#### 5.1.1. Model and parameters

A two-dimensional benchmark problem is calculated to verify the proposed NPSBFEM. A cantilever with one end fixed of length  $l$  and height  $h$  with a modulus of elasticity of  $E = 3 \times 10^4$  Pa and Poisson's ratio of  $\nu = 0.2$  in plane stress is examined (Fig. 4). The beam is subjected to a parabolic shear force of  $F = 7 \times 10^6$  N at the free end, and static analysis is performed. The values  $l/h = 3$  and  $l = 1.2$  m are selected.

The exact solution is expressed as shown in Eqs. (4-1) and (4-2), where the moment of inertia of the area is  $I = h^3/12$ ; then, the exact value of point A can be derived as  $u(A) = 0$  and  $v(A) = -2.695$  cm.

$$u(x, y) = \frac{Fy}{6EI} \left[ (9l - 3x)x + (2 + \nu) \left( y^2 - \frac{h^2}{4} \right) \right] \quad (4-1)$$

$$v(x, y) = -\frac{Fy}{6EI} \left[ 3\nu y^2(l - x) + (4 + 5\nu) \frac{h^2 x}{4} + (3l - x)x^2 \right] \quad (4-2)$$

#### 5.1.2. Methods and meshing

**5.1.2.1. PSBFEM.** The domain is discretized by 70 polygonal elements with 141 nodes, as shown in Fig. 5. The cantilever is simulated using the PSBFEM\_Area and PSBFEM\_Line functions. The Area function denotes the integration points over the area used for the integration, and the Line function denotes the points on the line that is used.

**5.1.2.2. PSBFEM and FEM.** To further verify the accuracy of NPSBFEM, the cantilever is also modeled using the commercial finite-element software ANSYS11.0. The PLANE42 element is

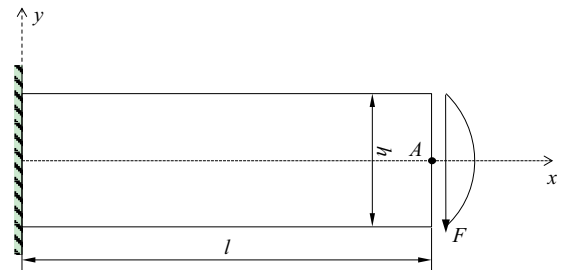


Fig. 4. Cantilever in plane stress.

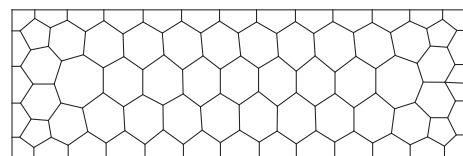


Fig. 5. Typical polygonal mesh with 70 polygons and 141 nodes.



selected, and the domain is discretized with 78 elements with 98 nodes (see Fig. 6). For comparison, the problem as calculated by PSBFEM\_Area is also presented.

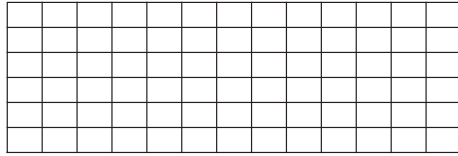


Fig. 6. Mesh with 78 elements and 98 nodes.

**Table 1**  
Displacement of point A.

Method	PSBFEM_Line	PSBFEM_Area	Exact
$u$ (cm)	$2.25 \times 10^{-5}$	$2.24 \times 10^{-5}$	0.0
$v$ (cm)	-2.6804	-2.6803	-2.695
Error (%)	0.542	0.545	–

**Table 2**  
Displacement of point A.

Method	FEM	PSBFEM_Area	Exact
$u$ (cm)	0.0	0.0	0.0
$v$ (cm)	-2.592	-2.656	-2.695
Error (%)	3.82	1.44	–

### 5.1.3. Results for the cantilever

**5.1.3.1. PSBFEM.** The displacements of point A for the different numerical methods are listed in Table 1. The results from the two methods correspond well and are close to the exact solution; the maximum error is only 0.545%. The results illustrate that the proposed approach can be used to simulate linear properties with high precision.

**5.1.3.2. PSBFEM\_Area and FEM.** The results of PSBFEM\_Area and FEM are listed in Table 2. The displacements of point A obtained using the two methods are close to the exact solution, and a higher precision is shown for the PSBFEM\_Area function.

## 5.2. Numerical simulation of a rockfill dam for elasto-plasticity

### 5.2.1. Model for calculation

To investigate the applicability of NPSBFEM in simulating elasto-plastic problems, the construction and impounding process of a concrete-faced rockfill dam (CFRD) with the extrusion-sidewall structure is simulated. The extrusion-sidewall is modeled with pentagonal elements, which are introduced for the transitions between cross-scale mesh. The dam studied in this research is symmetrical, with upstream and downstream slopes of 1 V:1.5 H, and the crest is 15 m. A plain-strain model consisting of 12,202 polygonal elements resulting in 25,702 DOFs is used. The corresponding model is shown in Fig. 7. Fig. 8 shows the material distribution of the dam and the size and location of the extrusion-sidewall. The technology of controlling the birth and death of elements is introduced into the program to simulate construction. The rockfill is divided into 79 layers, and the slab is constructed in one layer. Then, the water level is impounded to a 240 m elevation in thirty steps.

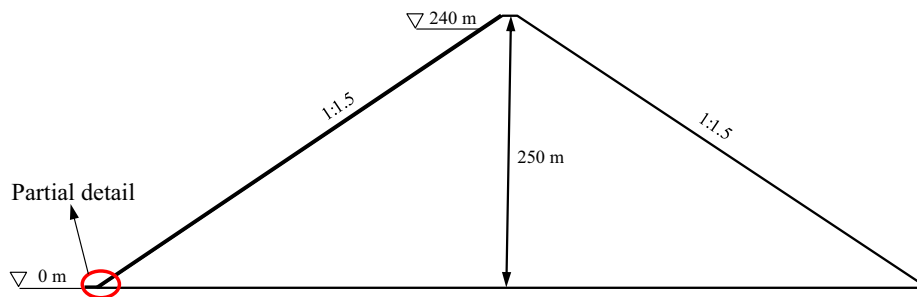


Fig. 7. Model of the CFRD.

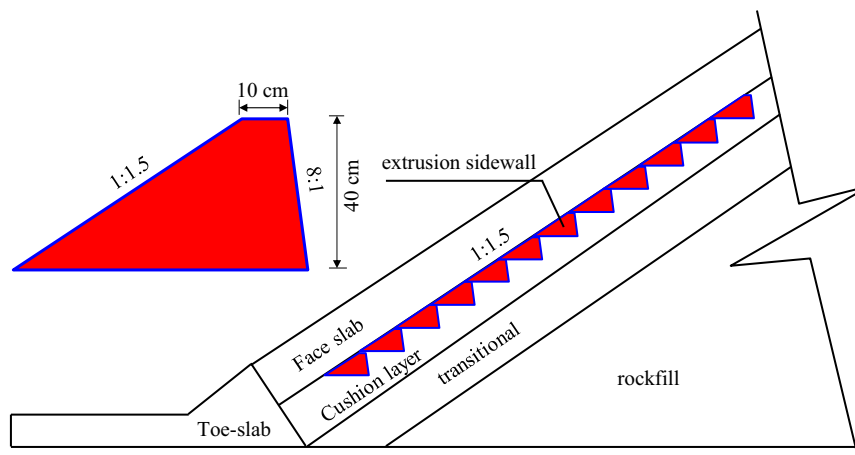


Fig. 8. Typical extrusion sidewall and partitioning of the dam body materials.

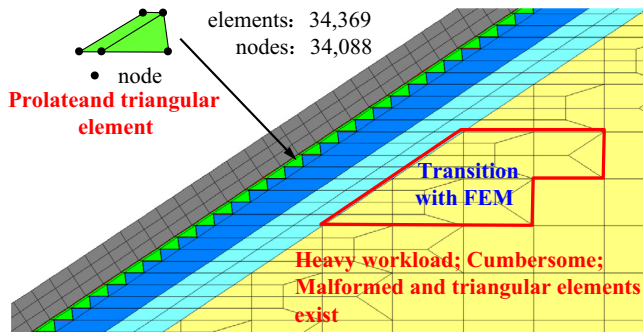


Fig. 9. The detail mesh of FEM.

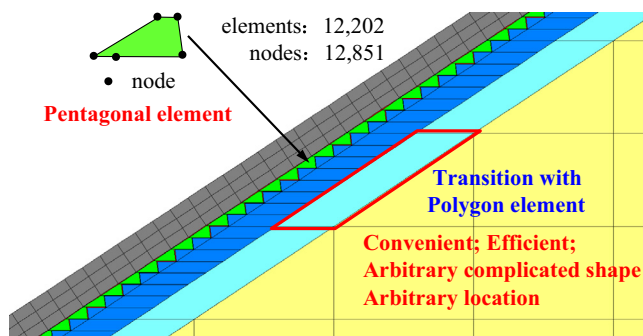


Fig. 10. NPSBFEM mesh detail.

**Table 3**  
Parameters of the linear elastic model.

Material	$\rho$ (g/cm <sup>3</sup> )	$E$ (MPa)	$\nu$
Slab	2.4	30,000	0.167

**Table 4**  
Parameters of the generalized plastic interface model [36].

$D_{s0}/\text{kPa}$	$D_{n0}/\text{kPa}$	$M_c$	$e_r$	$\lambda$	$a/\text{kPa}^{0.5}$	$b$	$c$
1000	1500	0.88	0.0	0.091	224	0.06	3.0
$\alpha$	$\gamma_d$	$k_m$	$M_f$	$k$	$H_0/\text{kPa}$	$f_h$	$t/m$
0.65	0.2	0.6	0.65	0.5	8500	2.0	0.1

**Table 5**  
Rockfill material parameters in the modified generalized plasticity model [38].

$G_0$	$K_0$	$M_g$	$M_f$	$\alpha_f$	$\alpha_g$	$H_0$	$H_{U0}$	$m_s$
1000	1400	1.8	1.38	0.45	0.4	1800	3000	0.5
$m_v$	$m_i$	$m_u$	$r_d$	$\gamma_{DM}$	$\gamma_u$	$\beta_0$	$\beta_1$	
0.5	0.2	0.2	180	50	4	35	0.022	

### 5.2.2. Element type

**5.2.2.1. Case 1.** The construction and impounding processes are simulated using the finite-element software GEODYNA. Quadrilateral isoparametric elements are used to model the slab and rockfill elements, and the interface elements between the slab and cushion layer as well as between the extrusion-sidewall and transitional are simulated using the Goodman element. To obtain a more accurate solution of the problem, a dense mesh is used in the FEM simulation, with 34,369 total elements and 34,088 nodes. The partial detail is illustrated in Fig. 9.

**5.2.2.2. Case 2.** The CEelement NPSBFEM (Gauss integration with the introduced Gaussian points) is selected as the slab and rockfill element type, and NPSBFEM is chosen to express the method presented in all figures. The interfaces between the slab and cushion layer as well as between the extrusion-sidewall and the transitional region are simulated by Goodman elements. To decrease the computational workload, the polygon elements are introduced to compose the cross-scale mesh between the cushion layer and rockfill, which leads to 12,202 elements and 12,851 nodes. The partial detailed mesh is shown in Fig. 10.

### 5.2.3. Parameter identification

A linear elastic model is used to model the concrete face slabs. According to the available engineering design information, the following properties are used in the analysis: a density  $\rho$  of 2.40 g/cm<sup>3</sup>, a modulus of elasticity  $E$  of 3e10 Pa, and a Poisson's ratio  $\nu$  of 0.167 (see Table 3). The modified generalized plastic interface model [35,36] is used to simulate the interface elements between the slab and rockfill; the model parameters are listed in Table 4. The generalized plasticity model [37,38] parameters of the rockfill are listed in Table 5.

### 5.2.4. Results and discussion

**5.2.4.1. Displacement and stress of the rockfill.** The displacement and stress of the rockfill after impoundment calculated using two dif-

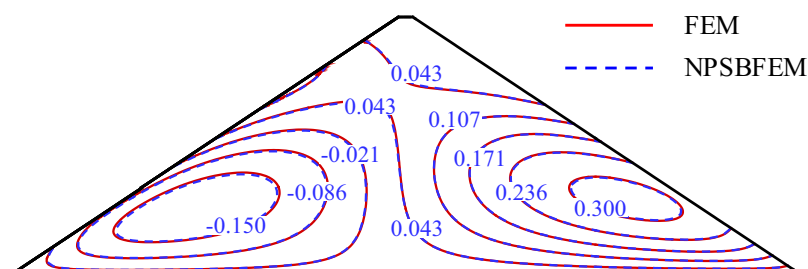


Fig. 11. Horizontal displacement of the rockfill after impoundment (units: m).

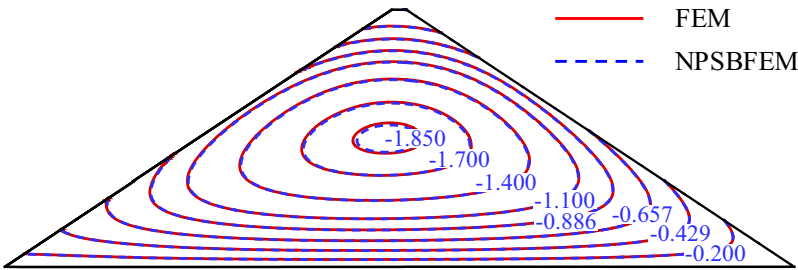


Fig. 12. Vertical settlement of the rockfill after impoundment (units: m).

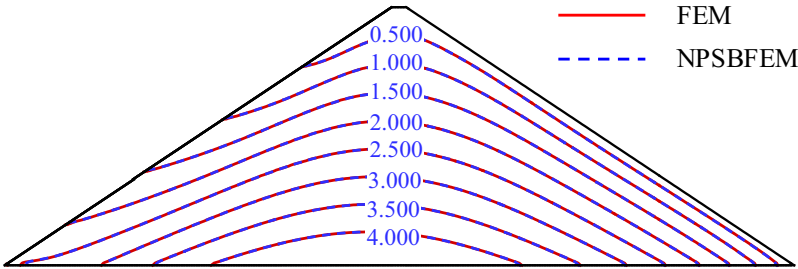


Fig. 13. Major principal stress of the rockfill after impoundment (units: MPa).

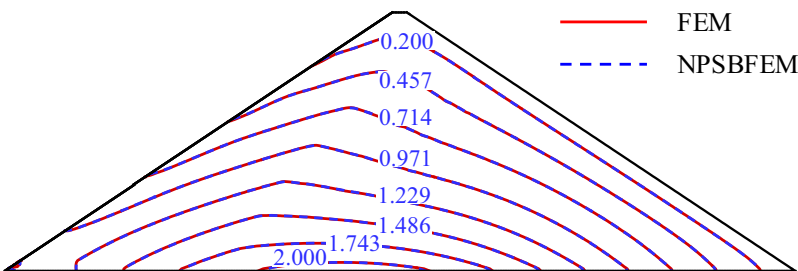


Fig. 14. Minor principal stress of the rockfill after impoundment (units: MPa).

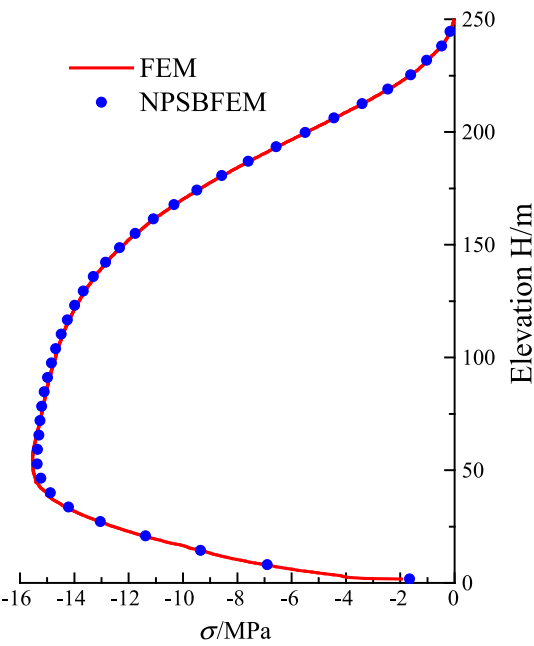


Fig. 15. Stress of the slabs along the slope direction after impoundment (units: MPa).

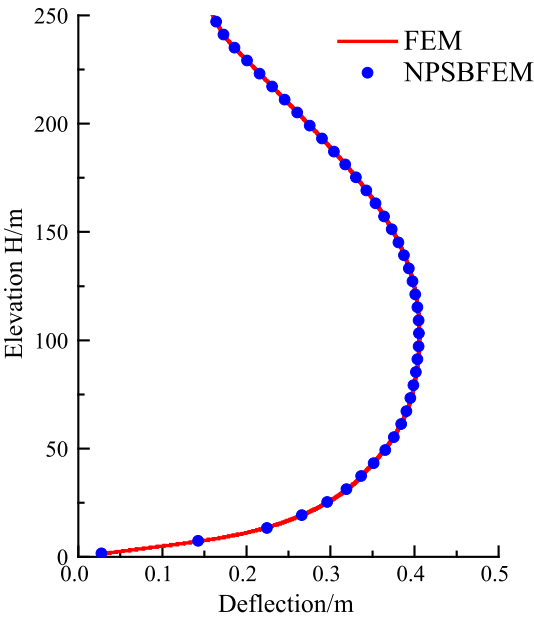


Fig. 16. The deflection of the slabs after impoundment (units: cm).



ferent methods are compared in Figs. 11–14. The results obtained with the two methods correspond well and exhibit only slight differences in partial locality; the discrepancy of the horizontal displacement is 0.18%, and the discrepancy of the vertical displacement is only 0.37%.

**5.2.4.2. Stress and settlement of the slab.** Fig. 15 shows the stress along the slope direction of the slab determined from conventional FEM, which corresponds well with the value obtained from NPSBFEM; the maximal discrepancy is less than 5%.

The vertical displacement of the slab after impoundment as simulated by the two methods are illustrated in Fig. 16. The maximum deflection, located at an elevation of approximately 103 m, is 40.6 cm.

## 6. Conclusions

According to the integral rule of triangular elements, a novel NPSBFEM is developed by introducing three internal Gaussian integration points over a subdomain covered by each line element in this paper. The nonlinear confirming shape function is constructed using the introduced Gaussian points by the semi-analytical solution derived from elastic theory. The NPSBFEM demonstrates a promising flexibility for more complex geometries without affecting its high level of precision.

Two numerical examples, a forcing analysis of a cantilever and a concrete face rockfill dam static analysis, are simulated using NPSBFEM. The exact displacements of the cantilever are derived to validate the method. Excellent agreement is achieved, with a maximum discrepancy of only 0.545%. The displacements and stresses are compared with a dense FEM mesh in the CFRD analysis. The differences in the displacements and stresses of the rockfill are less than 1% and 5%, respectively, and the results in the slab also correspond well with the FEM results. The results demonstrate that introducing internal Gaussian points is an acceptable alternative approach for extending scale boundary finite elements to analyze elasto-plastic problems.

PSBFEM can be extended to research and industry as a versatile and promising procedure for elasto-plastic analysis after its successful application in linear engineering problems. The potential significance of this method is expected to be confirmed in real-world applications. Extending the theory to three-dimensional structural analysis is imperative for the numerical simulation of complex engineering structures, particularly in a multi-scale context.

## Acknowledgements

This work was supported by the State Key Program of the National Natural Science Foundation of China (Grant No. 51138001) and the National Natural Science Foundation of China (Grant Nos. 51279025, 51379028). This financial support is gratefully acknowledged.

## Appendix A

### A. Generalized plasticity model for rockfill and generalized plastic interface model

The Pastor-Zienkiewicz model was developed by Pastor and Zienkiewicz [39,40] based on the basic framework of generalized plastic mechanics [41]. This model is applicable to the construction of civil engineering structures and seismic response analyses as well as the direct calculation of earthquake-induced permanent deformation. Several improvements to the generalized plasticity

model have been proposed in recent years [37,42,43]. In this study, the modified generalized plasticity model proposed by the authors [44] was used for the rockfill materials. The authors modified the shear modulus  $G$ , volume modulus  $K$ , load modulus  $H_L$ , and unload modulus  $H_U$  of this model:

$$G = G_0 p_a (p/p_a)^{m_s} \quad (1)$$

$$K = K_0 p_a (p/p_a)^{m_v} \quad (2)$$

$$H_L = H_0 \cdot p_a \cdot (p/p_a)^{m_l} \cdot H_f \cdot (H_v + H_s) \cdot H_{DM} \cdot H_{den} \quad (3)$$

$$H_u = \begin{cases} H_{u0} p_a (p/p_a)^{m_u} (\eta_u/M_g)^{-\gamma_u} & |\eta_u/M_g| < 1 \\ H_{u0} & |\eta_u/M_g| \geq 1 \end{cases} \quad (4)$$

$$H_{DM} = \exp((1 - \eta/\eta_{max})\gamma_{DM}) \quad (5)$$

$$H_{den} = \exp(\gamma d\epsilon_v) \quad (6)$$

where  $H_0$  is the coefficient of the plastic modulus,  $H_f$ ,  $H_v$  and  $H_s$  are the plastic coefficients,  $p_a$  is the atmospheric pressure, and  $\eta_{max}$  is the ratio of the maximum historical stress. The modified model can better describe the stress correlation and the cyclic hysteresis characteristics and has successfully calculated the static and dynamic response of CFRDs [38,45,46].

With the development of the elasto-plastic finite element analysis of CFRDs, the traditional Duncan-Clough hyperbolic and ideal elasto-plastic contact surface models have been unable to meet the needs of the elasto-plastic response analysis of CFRDs under seismic loads. Based on the framework of the generalized plasticity model and the two-dimensional interface model [47,48] proposed by Liu et al., Liu et al. developed a three-dimensional interface model [35] by combining the theory of the bounding surface model [45] with state-dependent theory [46]. In this model, a group of parameters can be used to accurately reflect the deformation characteristics of the interface, including shear dilation, shear contraction, hardening, softening and particle fracture, under monotonic and cyclic loading in three dimensions.

## References

- [1] Wachspress EL, Rohde SM. A rational finite element basis. Zürich: Academic Press Inc; 1976. doi: <http://dx.doi.org/10.1115/1.3452953>.
- [2] Dasgupta G. Interpolants within convex polygons: Wachspress' shape functions. J Aeronaut Eng 2003;16:1–8. doi: [http://dx.doi.org/10.1061/\(ASCE\)0893-1321\(2003\)16:1\(1\)](http://dx.doi.org/10.1061/(ASCE)0893-1321(2003)16:1(1)).
- [3] Shengyong D, Shao G. Integration scheme of Wachspress interpolation polygonal finite element method. J Southeast U Engl Ed 2013;43:216–20.
- [4] Ghosh S, Mallett RL. Voronoi cell finite elements. Comput Struct 1994;50:33–46. doi: [http://dx.doi.org/10.1016/0045-7949\(94\)90435-9](http://dx.doi.org/10.1016/0045-7949(94)90435-9).
- [5] Sukumar N, Moran B, Semenov Y. Natural neighbour galerkin method. Int J Numer Methods Eng 2001;50:1.
- [6] Dai KY, Liu GR, Nguyen TT. An n-sided polygonal smoothed finite element method (nSFEM) for solid mechanics. Finite Elem Anal Des 2007;43:847–60. doi: <http://dx.doi.org/10.1016/j.finel.2007.05.009>.
- [7] Mukherjee T, Webb JP. Hierarchical bases for polygonal finite elements. IEEE Trans Magn 2015;51:1–4. doi: <http://dx.doi.org/10.1109/TMAG.2014.2345497>.
- [8] Wang Z, Lu X. Macro-element approach based on mean value interpolation for solving potential problems. J Numer Methods Comput Appl 2007;28:179–87.
- [9] Sukumar N, Tabarraei A. Conforming polygonal finite elements. Int J Numer Methods Eng 2004;61:2045–66.
- [10] Sukumar N, Moran B, Belytschko T. The natural element method in solid mechanics. Int J Numer Methods Eng 1998;43:839–87. doi: [http://dx.doi.org/10.1002/\(SICI\)1097-0207\(19981115\)43:5<839::AID-NME423>3.0.CO;2-R](http://dx.doi.org/10.1002/(SICI)1097-0207(19981115)43:5<839::AID-NME423>3.0.CO;2-R).
- [11] Sukumar N, Malsch EA. Recent advances in the construction of polygonal finite element interpolants. Arch Comput Methods Eng 2006;13:129–63. doi: <http://dx.doi.org/10.1007/BF02905933>.
- [12] Wang Z. Advances in polygonal finite element method. Adv Mech 2006;36:344.
- [13] Chandler-Wilde SN, Langdon S. A Galerkin boundary element method for high frequency scattering by convex polygons. SIAM J Numer Anal 2007;45:610–40. doi: <http://dx.doi.org/10.1137/06065595X>.
- [14] Wolf JP, Schanz M. The scaled boundary finite-element method. Chichester, U. K: Wiley; 2004. doi: <http://dx.doi.org/10.1007/s00466-004-0556-2>.

- [15] Wolf JP, Song C. Finite-element modelling of unbounded media. Chichester, U. K: Wiley; 1996.
- [16] Wolf JP, Song C. The scaled boundary finite-element method – a primer: derivations. *Comput Struct* 2000;78:191–210. doi: [http://dx.doi.org/10.1016/S0045-7949\(00\)00099-7](http://dx.doi.org/10.1016/S0045-7949(00)00099-7).
- [17] Wolf JP, Song C. The scaled boundary finite-element method—a fundamental solution-less boundary-element method. *Comput Meth Appl Mech Eng* 2001;190:5551–68. doi: [http://dx.doi.org/10.1016/S0045-7825\(01\)00183-9](http://dx.doi.org/10.1016/S0045-7825(01)00183-9).
- [18] Bazyar MH, Song C. A continued-fraction-based high-order transmitting boundary for wave propagation in unbounded domains of arbitrary geometry. *Int J Numer Methods Eng* 2008;74:209–37.
- [19] Liu J, Lin G. A scaled boundary finite element method applied to electrostatic problems. *Eng Anal Boundary Elem* 2012;36:1721–32.
- [20] Liu J, Lin G, Li J, Zhong H. Analysis of quadruple corner-cut ridged square waveguide using a scaled boundary finite element method. *Appl Math Modell* 2012;36:4797–809.
- [21] Liu J, Zhang P, Lin G, Wang W, Lu S. Solutions for the magneto-electro-elastic plate using the scaled boundary finite element method. *Eng Anal Boundary Elem* 2016;68:103–14.
- [22] Liu J, Lin G, Li J. Short-crested waves interaction with a concentric cylindrical structure with double-layered perforated walls. *Ocean Eng* 2012;40:76–90.
- [23] Natarajan S, Ooi ET, Chiong I, Song C. Convergence and accuracy of displacement based finite element formulations over arbitrary polygons: LaPlace interpolants, strain smoothing and scaled boundary polygon formulation. *Finite Elem Anal Des* 2014;85:101–22. doi: <http://dx.doi.org/10.1016/j.finel.2014.03.006>.
- [24] Ooi ET, Song C, Tin-Loi F, Yang Z. Polygon scaled boundary finite elements for crack propagation modelling. *Int J Numer Methods Eng* 2012;91:319–42. doi: <http://dx.doi.org/10.1002/nme.4284>.
- [25] Ooi ET, Shi M, Song C, Tin-Loi F, Yang ZJ. Dynamic crack propagation simulation with scaled boundary polygon elements and automatic remeshing technique. *Eng Fract Mech* 2013;106:1–21. doi: <http://dx.doi.org/10.1016/j.engfracmech.2013.02.002>.
- [26] Ooi ET, Natarajan S, Song C, Tin-Loi F. Crack propagation modelling in functionally graded materials using scaled boundary polygons. *Int J Fract* 2015;192:87–105. doi: <http://dx.doi.org/10.1007/s10704-015-9987-3>.
- [27] Chiong I, Ooi ET, Song C, Tin-Loi F. Scaled boundary polygons with application to fracture analysis of functionally graded materials. *Int J Numer Methods Eng* 2014;98:562–89. doi: <http://dx.doi.org/10.1002/nme.4645>.
- [28] Bao Y, Hong Z, Gao L. Seismic fracture simulation of gravity dam based on polygon scaled boundary finite elements. *Water Res (Power)* 2015;4:72–5.
- [29] Mingguang S, Yanjie X, Hong Z. Modelling of crack propagation for composite materials based on polygon scaled boundary finite elements. *Eng Mech* 2014;7:1–7.
- [30] Lin Z, Liao S. The scaled boundary FEM for nonlinear problems. *Commun Nonlinear Sci Numer Simul* 2011;16:63–75. doi: <http://dx.doi.org/10.1016/j.cnsns.2010.03.005>.
- [31] Ooi ET, Song C, Tin-Loi F. A scaled boundary polygon formulation for elasto-plastic analyses. *Comput Methods Appl Mech Eng* 2014;268:905–37. doi: <http://dx.doi.org/10.1016/j.cma.2013.10.021>.
- [32] Pastor M, Zienkiewicz OC, Chan AHC. Generalized plasticity and the modelling of soil behaviour. *Int J Numer Anal Methods Geomech* 1990;14:151–90. doi: <http://dx.doi.org/10.1002/nag.1610140302>.
- [33] Zienkiewicz OC, Chan AHC, Pastor M, Schrefler BA, Shiomi T. Computational geomechanics. Chichester: Wiley; 1999.
- [34] Degao Z, Xianjing K, Bin X. User manual for geotechnical dynamic nonlinear analysis. Dalian: Institute of Earthquake Engineering, Dalian University of Technology; 2005.
- [35] Liu J, Zou D, Kong X. A three-dimensional state-dependent model of soil-structure interface for monotonic and cyclic loadings. *Comput Geotech* 2014;61:166–77. doi: <http://dx.doi.org/10.1016/j.compgeo.2014.05.012>.
- [36] Liu J, Kong XZD. Effects of interface models on deformation of interface between slab and cushion layer and slab stress of concrete faced rock fill dam. *J Geotech Eng* 2015;37:700–10 [Chinese].
- [37] Liu H, Zou D. Associated generalized plasticity framework for modeling gravely soils considering particle breakage. *J Eng Mech* 2013;139:606–15. doi: [http://dx.doi.org/10.1061/\(ASCE\)JEM.1943-7889.0000513](http://dx.doi.org/10.1061/(ASCE)JEM.1943-7889.0000513).
- [38] Zou D, Xu B, Kong X, Liu H, Zhou Y. Numerical simulation of the seismic response of the Zipingpu concrete face rockfill dam during the Wenchuan earthquake based on a generalized plasticity model. *Comput Geotech* 2013;49:111–22. doi: <http://dx.doi.org/10.1016/j.compgeo.2012.10.010>.
- [39] Pastor M, Zienkiewicz OC, Leung KH. Simple model for transient soil loading in earthquake analysis. II. Non-associative models for sands. *Int J Numer Anal Methods Geomech* 1985;9:477–98. doi: <http://dx.doi.org/10.1002/nag.1610090506>.
- [40] Pastor M, Zienkiewicz OC. A generalized plasticity, hierarchical model for sand under monotonic and cyclic loading. In: *Proc., 2nd international sym. numerical models in geomechanics*, Ghent. p. 131–49.
- [41] Mroz Z, Zienkiewicz OC. Uniform formulation of constitutive equations for clays and sands. *Mech Eng Mater* 1984;12:415–50.
- [42] Liu H. Unified sand modeling using associated or non-associated flow rule. *Mech Res Commun* 2013;50:63–70. doi: <http://dx.doi.org/10.1016/j.mechrescom.2013.04.003>.
- [43] Liu H, Zou D, Liu J. Constitutive modeling of dense gravelly soils subjected to cyclic loading. *Int J Numer Anal Meth Geomech* 2014;38:1503–18. doi: <http://dx.doi.org/10.1002/nag.2269>.
- [44] Zou D, Xu B, Kong X, Liu J, Zhou Y. Static and dynamic analysis of high concrete-faced rockfill dam based on generalized plastic model. *J Hydroelectr Eng* 2011;30:109–16.
- [45] Xu B, Zhou Y, Zou D. Numerical simulation on slabs dislocation of Zipingpu concrete faced rockfill dam during the Wenchuan earthquake based on a generalized plasticity model. *Scientificworldjournal* 2014;2014:572407. doi: <http://dx.doi.org/10.1155/2014/572407>.
- [46] Xu B, Zou D, Liu H. Three-dimensional simulation of the construction process of the Zipingpu concrete face rockfill dam based on a generalized plasticity model. *Comput Geotech* 2012;43:143–54. doi: <http://dx.doi.org/10.1016/j.compgeo.2012.03.002>.
- [47] Liu H, Ling HI. Constitutive description of interface behavior including cyclic loading and particle breakage within the framework of critical state soil mechanics. *Int J Numer Anal Meth Geomech* 2008;32:1495–514. doi: <http://dx.doi.org/10.1002/nag.682>.
- [48] Liu H, Song E, Ling HI. Constitutive modeling of soil-structure interface through the concept of critical state soil mechanics. *Mech Res Commun* 2006;33:515–31. doi: <http://dx.doi.org/10.1016/j.mechrescom.2006.01.002>.